How to Cite: Liu, X., Bekchanov, D., Baikenov, M.I., & Su, X. (2024) Construction of Ag/AgCl@MIL-53(Fe): Achieving Efficient Photocatalytic Water Oxidation via the Plasma-Phase Silver and Heterojunction Synergistic Effect. *Eurasian Journal of Chemistry, 29, 3(115), 160-170.* https://doi.org/10.31489/2959-0663/3-24-14

Article

Received: 2 July 2024 | Revised: 22 August 2024 |
Accepted: 9 September 2024 | Published online: 23 September 2024

UDC 544.47+542.943

https://doi.org/10.31489/2959-0663/3-24-14

Xiaofei Liu[1], Davronbek Bekchanov[2], Murzabek I.Baikenov[3], Xintai Su[4]*

[1]*College of Chemistry and Chemical Engneering, Xinjiang Agricultural University, Urumqi, China;*
[2]*Faculty of Chemistry, Department of Polymer Chemistry, National University of Uzbekistan, Tashkent, Uzbekistan;*
[3]*Karaganda Buketov University, Karaganda, Kazakhstan;*
[4]*School of Environment and Energy, Guangdong Provincial Key Laboratory of Solid Wastes Pollution Control and Recycling, South China University of Technology, Guangzhou, Guangdong, China*
*(*Corresponding author's e-mail: suxintai@scut.edu.cn)*

Construction of Ag/AgCl@MIL-53(Fe): Achieving Efficient Photocatalytic Water Oxidation via the Plasma-Phase Silver and Heterojunction Synergistic Effect

The development of highly efficient water oxidation catalysts is a bottleneck in achieving artificial photosynthesis, as water oxidation is a complex process involving multiple electron and proton transfers. To further improve the photocatalytic water oxidation performance of MIL-53(Fe), a series of Ag/AgCl@MIL-53(Fe) samples with different Fe:Ag ratios were synthesized by hydrothermal methods and used in the photocatalytic water oxidation reactions. XRD characterization showed the successful preparation of Ag/AgCl@MIL-53(Fe) heterostructure catalysts. The reaction results showed that sample AAM-2 (Fe:Ag=5:1) had the best photocatalytic water oxidation performance, with the highest TOF value of 0.14 mmol/(g·s) and quantum efficiency of 39.0 % under the conditions of catalyst mass of 1 mg and pH=9.0 for boric acid-borax buffer solution. Measurements of photocurrent indicated that the AAM-2 samples doped with Ag/AgCl had higher photocurrent densities, thus improving the photocatalytic performance. This provides new insights for constructing highly efficient porous MOFs catalysts.

Keywords: Metal organic framework (MOFs); hydrothermal method; MIL-53(Fe); Ag/AgCl@MIL 53(Fe); surface plasma resonance; heterojunction; photocatalysis of water oxidation; photocurrent densities.

Introduction

Photocatalytic water splitting, as an advanced technology, has a very broad application prospect in the field of energy. Its core value is that it can efficiently convert sunlight into chemical energy, thus realizing the direct decomposition of water and producing clean hydrogen and oxygen [1]. This catalytic process can not only reduce the dependence on fossil fuels and reduce environmental pollution, but also has far-reaching significance in promoting the sustainable development of energy. It consists of two half-reactions: the oxidation of water to O_2 and the reduction of hydrogen ions to H_2. Compared with the reduction of water with two electrons transferred, the oxidation of water is more difficult to occur because it involves the transfer of four electrons and the formation of an O–O bond [2]. Therefore, the water oxidation reaction process is more complex and challenging than the water reduction reaction.

Previous studies have explored metal oxides, metal sulfides, and other materials as photocatalysts for water oxidation [3–4]. However, the application of Metal-Organic Frameworks (MOFs) in this respect is less common, mainly because most MOFs cannot withstand the harsh conditions of water oxidation. Lin et al. reported the three UiO-67 catalysts doped with Ir, which showed high water oxidation activity [5]. However, due to the extreme conditions of water oxidation, the MOFs catalysts were unstable, which led to the partial decomposition of Ir complexes. Moreover, the Ir based composites are neither economical. It is worthwhile to explore the development of stable, cost-effective MOFs as photocatalysts for water oxidation. Iron is a resource-rich element, and many MOFs materials containing iron MOFs, such as MIL-53(Fe) and MIL-88 (Fe), have specific structures and uniform sizes. In previous studies, the iron oxygen clusters Fe-O within iron-based MOFs could be excited under visible light, leading to their visible light response characteristics [6]. Therefore, many iron-based MOFs have been used in photocatalytic reactions. Kholdeeva et al. investigated the capability of iron-based metal-organic frameworks MIL-100 and MIL-101 for carbon-hydrogen oxide formations [7]. Wang et al. have synthesized both MIL-100(Fe) and MIL-68(Fe), and found that they can achieve selective hydroxylation of benzene to phenol with high selectivity [8].

Introducing another metal ion to prepare bimetallic MOFs is one of the modification methods to improve the performance of single-metal MOFs [9]. Due to the significant amplified absorbance of the surface plasma resonance (SPR) of noble metal nanoparticles in the visible light region, it is possible to modify the photocatalyst [10]. Particularly, Ag/AgX (X = Cl, Br), a type of composite plasma photocatalyst, can generate highly active photo-excited carriers under visible light irradiation to achieve the rapid degradation of various organic pollutants [11–12]. Additionally, Ag/AgX modification has significantly enhanced the photocatalytic reaction activity of traditional semiconductor photocatalysts such as TiO_2, $BiVO_4$, Bi_2WO_4 and C_3N_4 [14]. Since the silver nanoparticles exhibit a plasma resonance effect that can introduce a new light absorption source and possesses an energy-matched band structure, it can improve the efficiency of carrier separation.

However, whether the additive Ag/AgX can enhance the photocatalytic performance of MOFs and whether the role of Ag/AgCl in photocatalytic reactions based on MOFs systems is similar to that previously reported in inorganic semiconductor systems is still an open question. Therefore, the study of the photocatalytic process of Ag/AgX@MOFs is of great significance. Previous studies have shown that MIL-53(Fe) can improve its photocatalytic water oxidation performance by doping metal ions. In this article, the effective combination of the plasma Ag/AgCl with MIL-53(Fe) has improved the photocatalytic water oxidation performance of MIL-53(Fe) through the heterojunction mechanism. This structure is conducive to the synergistic transfer of photogenerated electrons and holes in the catalyst. The research results on photocatalytic water oxidation by Ag/AgCl@MIL-53(Fe) will provide new ideas for the design and development of high-efficiency MOFs-based photocatalysts.

Experimental

Preparation of Ag/AgCl@MIL-53(Fe) Catalysts

Different samples with varying Fe/Ag molar ratios were prepared using a hydrothermal method. A mixture of 10 mmol of 1,4-H_2BDC (AR), an appropriate amount of $FeCl_3 \cdot 6H_2O$ (AR) and $AgNO_3$ (AR), and 50 mL of DMF (SP) solution was prepared, and the mixture was stirred at room temperature for 30 min. The obtained precipitates were then transferred into a sealed 100 mL autoclave, and the system was heated at 150 °C for 12 h. After the reaction, the autoclave was allowed to cool to room temperature naturally, and the obtained precipitates were washed with DMF three times, followed by water washing three times, and further dried under vacuum at 80 °C for 12 h to obtain the final Ag/AgCl@MIL-53(Fe) photocatalyst. The molar ratio of Fe to Ag was varied, while maintaining the total molar ratio of metal ions to ligand as 1:1. Based on the molar ratio compositions, the resulting samples were labeled as AAM-0 (Fe:Ag = 1:0), AAM-1 (Fe:Ag = 7:1), AAM-2 (Fe:Ag = 5:1), and AAM-3 (Fe:Ag = 2:1).

Catalyst Characterization

X-ray diffraction patterns (XRD) were determined on a Bruker AXS D8 Focus diffractometer (operated at 40 kV and 30 mA) using Cu Kα irradiation.

N_2-BET was performed using a ST-08B physical-sorption instrument at 77 K.

Fourier transform infrared (FT-IR) spectra were recorded on an Equinox55 spectrometer (Bruker, Germany) by means of the KBr pellet technique.

Scanning electron microscope (SEM) images of the typical samples were recorded on a SU8010 model supplied by Hitachi Ltd. of Japan. Before conducting the SEM test, a layer of Au was sprayed onto the surface of the sample to enhance its conductivity. When performing mapping tests, the solid sample was dispersed in anhydrous ethanol and ultrasonically dispersed before being evenly dripped onto a silicon wafer on an optical surface for testing.

Synthesis of the Photosensitiser $[Ru(bpy)_3](ClO_4)_2$

Studies have shown that in a photocatalytic water oxidation system using $[Ru(bpy)_3]^{2+}$ as the photosensitizer, $[Ru(bpy)_3](ClO_4)_2$ is more conducive to the photocatalytic water oxidation reaction than $[Ru(bpy)_3]Cl_2$. Therefore, configuring the original photosensitiser $[Ru(bpy)_3]Cl_2$ into $[Ru(bpy)_3](ClO_4)_2$ is beneficial for enhancing the photocatalytic oxygen production performance of the catalyst.The specific steps are as follows: Dissolve 400 mg of $[Ru(bpy)_3]Cl_2$ in a small amount of distilled water to ensure complete dissolution, transfer to a 50 mL opaque reaction flask, and then add 4 M $HClO_4$ acid solution dropwise under magnetic stirring until no more white precipitate is formed. The solution is filtered and washed three times with ether to remove H^+ ions and water from the precipitate, which is then dried in the dark at room temperature for 12 h. And storing the obtained final product $[Ru(bpy)_3](ClO_4)_2$ orange powder in the dark at low temperature.

Evaluation of Photocatalytic Oxygen Production Performance

In the non-homogeneous system for photocatalytic water oxidation experiments, the synthesized samples were used as photocatalysts for water oxidation (0–2 mg), with $[Ru(bpy)_3](ClO_4)_2$ serving as the photosensitiser (1.0 mM, 8.76 mg), and $Na_2S_2O_8$ as the electron sacrificial agent (40 mM, 95.2 mg). The reactions were carried out in a borax-borate buffer solution (80 mM, pH = 8.0–10.0). The specific steps were as follows: first, a certain amount of catalyst, photosensitiser, and electron sacrificial agent were weighed in the dark, and then added separately to the reactor, followed by the addition of a 10 mL of buffer solution using a pipette gun. The sampling bottle was sealed and subjected to gas displacement treatment. The photocatalytic reaction was carried out using PLS-SXE xenon lamp (300 W) produced by Porfilet as the light source. Before beginning the use of the xenon lamp (with a 420 nm filter), use a power meter to set the light power density of the xenon lamp to 100 mW/cm^2 (simulating the solar irradiance). Place the sampling bottle that has been air-exhausted under the adjusted xenon lamp, and perform magnetic stirring simultaneously. Every two minutes, a gas sampling needle with a capacity of 250 μL is used to withdraw 100 μL of the gas from the sampling bottle and inject it into the GC-2014C gas chromatography produced by Shimadzu, Japan. To detect the oxygen content generated within the bottle, O_2 (99.99 %) is used as the standard sample for quantification, and the oxygen production is calculated based on the peak area of oxygen measured each time. In this experiment, sampling continues until 10 minutes, until the peak area of oxygen no longer increases. Additionally, use a pH meter to measure the pH value of the solution after the complete reaction.

Photoelectrochemical Performance Test

The preparation steps for the electrode are as follows: Take 8 mg of the catalyst, disperse it in approximately 1 mL of ethanol, add 40 μL of Nafion solution, and sonicate to form a paste. The paste is then spin-coated uniformly on a 1 cm × 1 cm FTO conductive glass sheet, and dried in a vacuum at 110 °C for 12 h to prepare the working electrode. After that, platinum wire is used as the counter electrode, and Sure enough electrode is used as the reference electrode, with 80 mM $Na_2S_2O_8$ solution as the electrolyte. Photocurrent measurements are performed using a 300W xenon lamp as the light source. The current response changes of different samples under illumination/non-illumination conditions are achieved through intermittent illumination over a fixed time.

Results and Discussion

X-ray diffraction (XRD) was used to analyze the phase composition of the Ag/AgCl@ MIL-53(Fe)(AAM) sample. As shown in Figure 1, the characteristic peaks of the pure phase AAM-0 appeared at 9.4°, 12.7°, 17.6°, and 25.4°, which matched the XRD patterns of the simulated crystal of MIL-53(Fe) reported previously. The XRD spectrum of the AAM-2 sample, which had been doped with Ag/AgCl, was mainly dominated by the characteristic peaks of MIL-53(Fe). In addition, the diffraction peaks corresponding to the cubic phase AgCl (111), (200), and (220) faces were observed, located at 27.8°, 32.3°, and 46.3°, respectively. A weak peak was also observed at 38.2° in the XRD spectrum of AAM-2, corresponding to the (111) plane of the cubic phase metallic Ag [14]. This indicates that the Ag/AgCl heterojunction structure was successfully introduced. It is noteworthy that the position of the characteristic diffraction peaks of MIL-53(Fe) in the AAM-2 spectrum did not change significantly, indicating that doping with Ag/AgCl would not destroy the crystal structure of MIL-53(Fe).

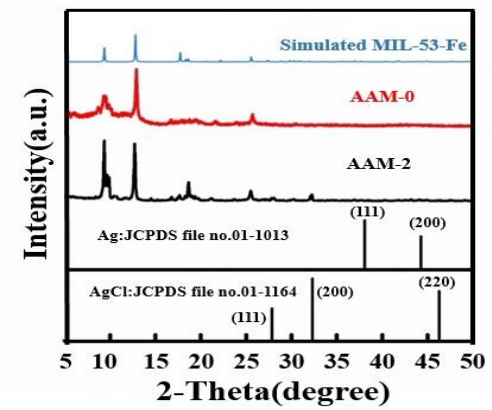

Figure 1. XRD patterns of AAM-0 and AAM-2

The BET-BJH method was used to analyze the specific surface area, pore volume, and pore diameter of the AAM-0 and AAM-2 catalysts, with the results listed in Table 1. The synthesized AAM-0 and AAM-2 samples had specific surface areas of 52 and 28 m^2/g, respectively. After doping with Ag/AgCl, the specific surface area decreased, suggesting that Ag/AgCl may block the pores of the MIL-53(Fe). The adsorption isotherms are shown in Fig. 2, where both the AAM-0 and AAM-2 catalysts exhibit IV-type isotherms and H3-type hysteresis loops. Additionally, with an average particle size of 3.0 nm for AAM-0 and 3.3 nm for AAM-2. According to the IUPAC classification of pores, it is evident that they predominantly consist of mesopores, which are generated by the agglomeration of particles. The average pore diameter of the AAM-2 sample with Ag/AgCl doping is smaller than that of the AAM-0 sample.

Table 1

Textural properties of the catalysts

Sample	Specific surface area (m^2/g) [a]	Average pore volume ($cm^3\ g^{-1}$)[b]	Average pore size (nm) [c]
AAM-0	52	0.09	3.0
AAM-2	28	0.06	3.3
[a]Calculated by the BET method. [b] BJH desorption pore volume. [c] BJH desorption average pore diameter.			

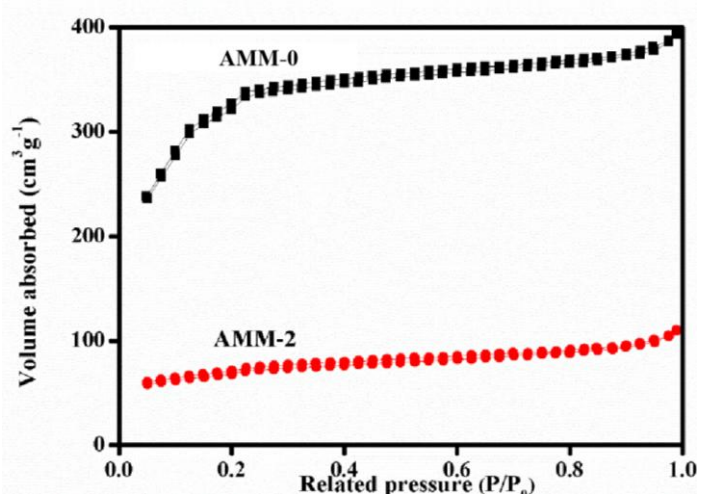

Figure 2. Adsorption curves of AAM-0 and AAM-2

The nanocrystalline structure of AAM was further determined by scanning electron microscopy (SEM). Fig. 3 shows the SEM morphologies of the AAM-0 and AAM-2 catalysts, where the pure phase AAM-0 appears to have a tetragonal structure, indicating the successful synthesis of MIL-53(Fe), which is consistent with the XRD results. Additionally, it was observed that the AAM-2 samples doped with Ag/AgCl still maintained a framework structure. However, in comparison to the tetragonal structure of AAM-0, there is a noticeable change in the microscopic structure, with the framework structure appearing less clear and distinct.

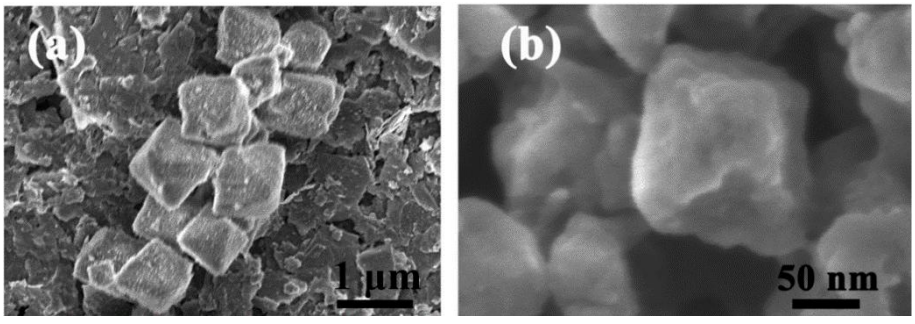

Figure 3. SEM images of (a) AAM-0 (b) AAM-2

Furthermore, the molecular structure of the AAM-0 and AAM-2 catalysts was investigated using infrared spectroscopy (Fig. 4). It was found that the infrared spectra of the AAM-2 sample were very similar to those of the AAM-0 sample. The characteristic absorption peaks at 1536 and 1392 cm^{-1} were attributed to the asymmetric stretching vibration of the carboxyl group (υ_{as} (C-O)) and the symmetric stretching vibration (υ_{s} (C-O)) [15], respectively, indicating the presence of dicarboxylate linkers in the framework. The characteristic absorption bands of the benzene ring were observed at 1629 cm^{-1} (C=C) and 756 cm^{-1} (C-H) [16]. Additionally, the band at 542 cm^{-1} in the low-frequency region also confirmed the typical Fe-O stretching vibration found in the framework [17].

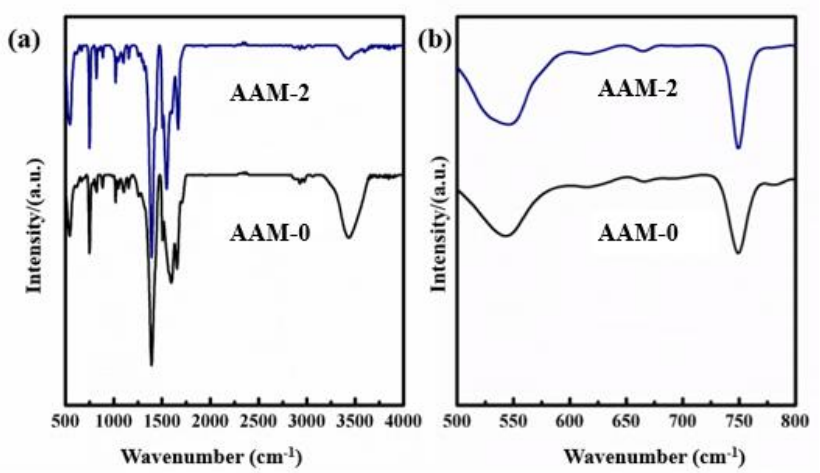

Figure 4. FT-IR spectra of as-prepared AAM-0 and AAM-2 samples

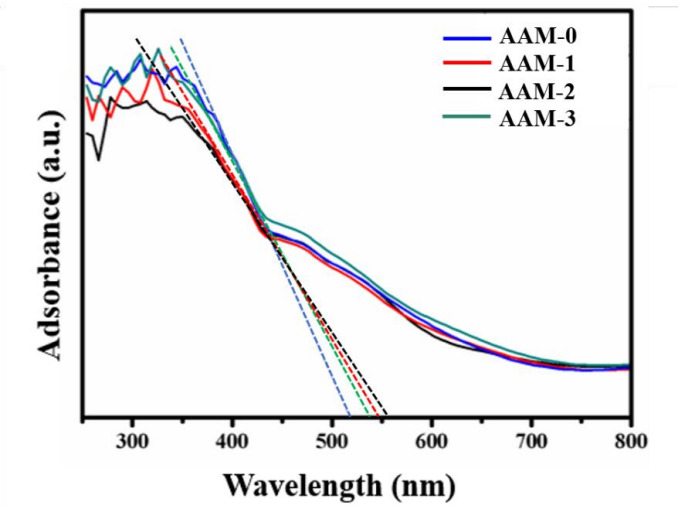

Figure 5. UV-vis diffuse reflectance spectra of AAM-0, AAM-1, AAM-2 and AAM-3 samples

The spectral absorption capability of the catalysts for visible light has been investigated through the determination of the ultraviolet-visible diffuse reflection spectra (URS) of the samples. As shown in Fig. 5, the absorption onset for Fe-MIL 53 is approximately 517 nm. As the amount of Ag/AgCl doping increases, the absorbance in the visible light region (>400 nm) is enhanced compared to Fe-MIL 53, with the maximum absorption intensity achieved when the Fe:Ag ratio is 5:1 (AAM-2). An increase in the absorbance in the visible light region implies a higher utilization efficiency of solar energy. Therefore, incorporating Ag/AgCl into Fe-MIL 53 particles can enhance its photocatalytic water oxidation performance.

To compare the influence of the loading of Ag/AgCl on photocatalytic activity, we performed tests on the oxygen production activity of AAM-0, AAM-1, AAM-2 and AAM-3 catalysts under the same conditions of water photolysis. First, a control experiment was conducted under conditions without light or catalyst, and no O_2 was detected, indicating that the O_2 came from the photo-oxidation of water. The curves of oxygen

production versus time for the four photocatalysts, AAM-0, AAM-1, AAM-2, and AAM-3, under visible light are shown in Fig. 6. All four samples exhibited photocatalytic activity for water oxidation, with the AAM-0 catalyst producing 20.16 μmol of oxygen in 10 min. The oxygen production of the AAM photocatalysts was improved, with AAM-2 (Fe:Ag = 5:1) producing 45.86 μmol of oxygen in 10 min, which is 2.27 times that of MIL-53(Fe). This result indicates that under the same preparation conditions, the loading of Ag/AgCl effectively improves the photocatalytic activity of MIL-53(Fe).

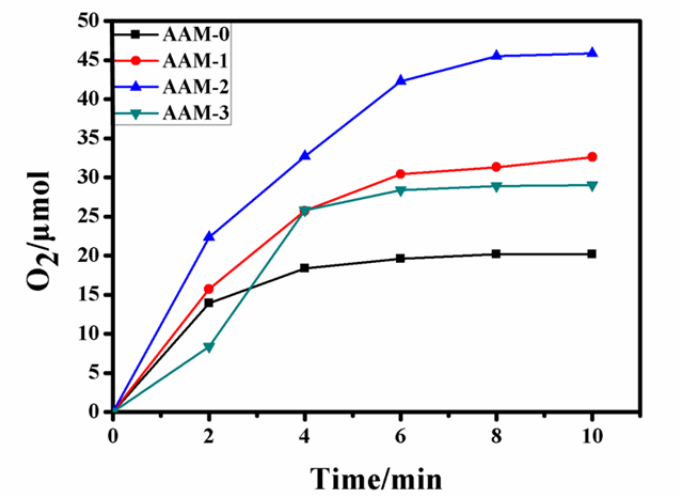

Figure 6. Kinetics of oxygen generation of the photocatalytic system with different loads of Ag/ AgCl based MIL-53(Fe)

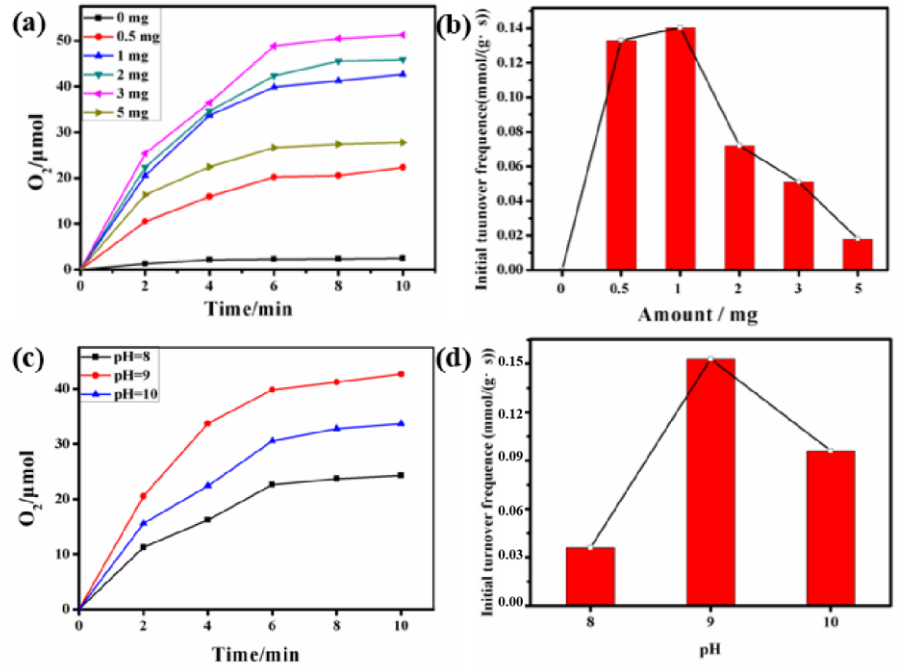

Figure 7. Kinetics of O_2 evolution of the photocatalytic system using AAM-1(Fe:Ag=5:1). (*a*) using different amountof AAM-2, (*b*) initial turnover frequencies of AMM-1 using different amount, (*c*) at different pH, (*d*) initial turnover frequencies at different pH

To further screen the conditions of the photocatalytic water oxidation system, the selected AAM-2 (Fe:Ag=5:1) was tested for its photocatalytic water oxidation performance under different conditions. From Fig 7, we can see that under the condition without light or catalyst, there is only a very small amount of oxygen in the system, and no oxygen generation is observed. The experimental results show that the AAM-2 (Fe:Ag=5:1) catalyst plays a major role in the photocatalytic water oxygenation reaction. At a pH of 9.0,

with the increase in the amount of catalyst, the oxygen production also increases, reaching a maximum value of 50.12 μmol when the catalyst reaches 3 mg. However, when the amount of catalyst increases to 5 mg, the oxygen production decreases. This indicates that adding more catalyst does not necessarily mean better performance, as excessive catalyst can adsorb on the surface of the photosensitizer, hindering direct contact between the photosensitizer and light, and also affecting the catalytic activity of the catalyst. At 1 mg of catalyst, the TOF value is 0.14 mmol/(g·s), with the highest oxygen production efficiency, and 1 mg is selected as the optimal amount of catalyst. When further increasing the amount of catalyst, the photocatalytic activity may actually decrease. This could be due to the excessive addition of the catalyst, which may reduce the transparency of the system, inhibit the contact between the photosensitizer and light, and thus lower the catalytic efficiency. After the reaction, the solution color changed from orange-yellow to dark-brown. The pH of the solution was measured, and it was found to have decreased from 9 to 8.5. The rate-controlling step of the photo-catalytic oxygen production reaction is given by formula (1). The accumulation of H^+ leads to a continuous decrease in pH, indicating that $[Ru(bpy)_3]^{3+}$ is not consumed in time. This will cause the reaction solution to change color and terminate the reaction.

$$4[Ru(bpy)_3]^{3+} + 2H_2O \rightarrow 4[Ru(bpy)_3]^{2+} + O_2 + 4H^+ \quad (1)$$

To further screen the optimal conditions, the effects of different pH values of boric acid buffer solutions on the photocatalytic water oxidation performance of AAM-2 catalyst were explored, as shown in Fig. 7(*c*). In alkaline conditions, there is a significant difference in the amount of oxygen released under different pH values. At pH = 8.0, the oxygen production is 19.8 μmol, and at pH = 10.0, the oxygen production is 32.42 μmol. Generally, high pH solutions are favorable for water oxidation because they can remove H^+ generated during the catalytic process [18], as shown in equation (1). This may be due to the structural decomposition of AAM-2 MOFs in strong alkaline solutions. This also indicates that the optimal pH for AAM-2 photocatalytic water oxidation is 9.0.

The initial quantum efficiency of the AAM-2 sample under the optimal reaction conditions was also calculated as follows:

The oxygen production amount in the initial 1 min was: 14.4 μmol

The number of consumed photons $= 14.4 \times 10^{-6} \times 6.02 \times 10^{23} \times 4$

$= 3.46 \times 10^{19}$

The optical power measured by the power meter: P=100 mW/cm^2, the diameter of the reaction bottle is 2 cm, The height of the liquid level in the bottle is 3.5 cm.

The light energy per minute: $E = P \times t \times D \times h$

$= 100 \times 10^{-3} \times 60 \times 2 \times 3.5$ J

$= 42$ J

The energy of a single photon: $E_{ph} = h\nu = \frac{hc}{\lambda} = \frac{6.34 \times 10^{-34} \times 3 \times 10^8}{420 \times 10^{-9}}$

$= 4.73 \times 10^{-19}$ J

The total number of photons provided by the light per minute: $= \frac{E}{E_{ph}} = \frac{42}{4.73 \times 10^{-19}} = 8.88 \times 10^{19}$

Initial quantum efficiency:

$$\Phi_{QY(initial)} = \frac{\text{The number of photons consumed in the production of oxygen}}{\text{The total number of photons provided by the light per second}}$$

$$= \frac{3.46 \times 10^{19}}{8.88 \times 10^{19}} \times 100\ \%$$

$= 39.0\ \%$

A cyclic experiment using the catalyst to examine the stability of the catalyst in the photocatalytic water oxidation process (Fig. 8). The AAM-2 catalyst synthesized by the water heat method (Fe:Ag = 5:1) was recycled for testing the catalytic performance of the water oxidation reaction. The recycled catalyst still showed good catalytic activity, but the amount of oxygen produced in the cyclic reaction showed a slight decrease. The possible reason for this result is that the catalyst will be physically lost during the recovery process, which will affect the cycle reaction.

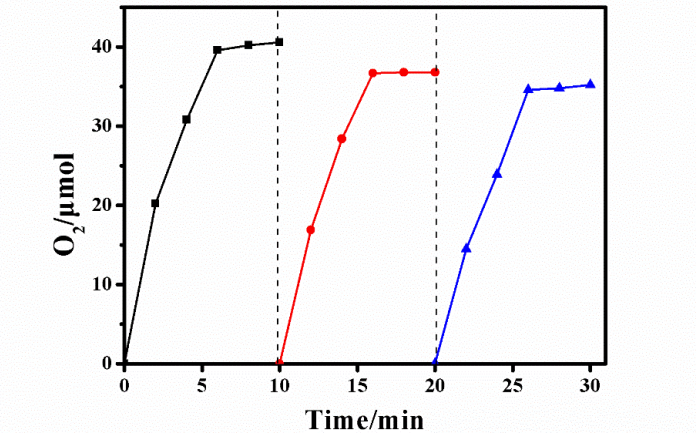

Figure 8. Cyclic behavior of AAM-2 (Fe:Ag=5:1) photocatalystic water oxidation

To further understand the electrochemical performance of the catalyst, the photocurrents of the AAM-0 and AAM-2 samples were measured, as shown in Fig. 9. It can be observed that the photocurrent density of AAM-2 is significantly higher than that of the pure phase AAM-0. This increase in photocurrent density is related to the effective separation of photogenerated electron-hole pairs, indicating that the catalyst doped with Ag/AgCl can enhance its photocurrent density, suggesting a higher efficiency of separation of photogenerated electron-hole pairs and thus improved photoelectrochemical performance.

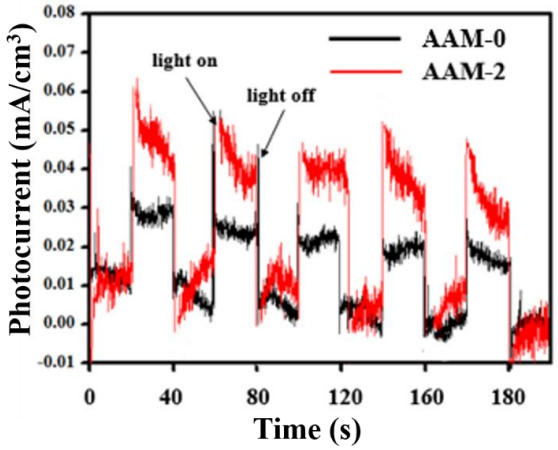

Figure 9. Transient photocurrent response of AAM-0, and AAM-2

Based on the results and discussion above, an hypothesis of the photocatalytic reaction pathway in the Ag/AgCl@MIL-53(Fe) system was proposed (Fig. 10). The conduction band (CB) and valence band (VB) energies of MIL-53(Fe) were 0.50 eV and 2.09 eV, respectively, with a bandgap energy of 2.59 eV, capable of being excited under visible light. Since the VB value of MIL-53(Fe) is higher than that of the water oxidation-reduction potential, MIL-53(Fe) is able to catalyze the water oxidation reaction under visible light irradiation [18]. For Ag/AgCl, due to its larger bandgap of 3.26 eV, AgCl cannot be excited by visible light. Upon irradiation with visible light, the Ag plasmon is excited, transferring the plasmon-induced electrons into the CB of AgCl. The positive charge in the Ag region can recombine with the photogenerated electrons in MIL-53(Fe), effectively promoting the separation of charge carriers in MIL-53(Fe). The oxidation of H_2O on MIL-53(Fe) by photogenerated electrons and holes migrate cooperatively in the Ag/AgCl@MIL-53(Fe) system, ensuring the longevity of the charge carriers and enhancing the photocatalytic activity. Importantly, MIL-53(Fe) as a typical metal-organic framework possesses a large surface area and high porosity. This structural feature endows Ag/AgCl@MIL-53(Fe) with open channels for effective diffusion and regulation of reactants, which is conducive to the photocatalytic reaction.

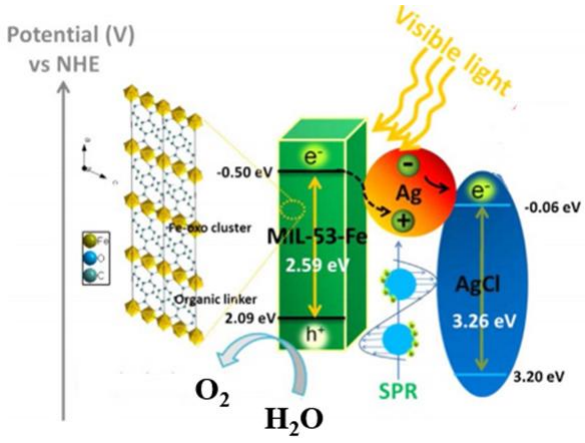

Figure 10. Proposed photocatalytic water oxidation reaction pathway of Ag/AgCl@MIL-53(Fe) under visible light irradiation

Conclusions

Hydrothermal synthesis of Ag/AgCl doped in MIL-53(Fe) for the study of photocatalytic water oxidation. The photocatalytic water oxidation performance was optimized by adjusting the Fe:Ag ratio. XRD results showed the successful preparation of the Ag/AgCl@MIL-53(Fe) heterostructure catalyst. According to the measured photocatalytic water oxidation performance, when the Fe:Ag ratio was 5:1, the photocarrier separation efficiency of sample AAM-2 was the highest, and its corresponding photocatalytic oxygen production performance was also the best among a series of Ag/AgCl@MIL-53(Fe) samples, which showed a clear advantage compared to the oxygen production performance of the pure phase MIL-53(Fe). Moreover, it exhibited good stability. Photocurrent test results indicated that under strong oxidative conditions, the AAM-2 catalyst had structural stability and could maintain a stable internal photoresponse current. The calculated results obtained a quantum efficiency of 39.0 % for AAM-2, with a TOF value of 0.14 mmol/(g·s). This has certain scientific guidance significance for enhancing the MOFs-based catalysts in photocatalytic water oxidation reactions.

Funding

The authors acknowledge deeply the financial supporting by the project of the Xinjiang Science and Technology Department (2022B01042, 2022E01051, 2022E02098), the Yili State Science and Technology Bureau Project (YZ2023A7, YZD2024A16, YZ2023A11), and the Project of Changji Science and Technology Bureau (2023Z04)

*Author Information**

**The authors' names are presented in the following order: First Name, Middle Name and Last Name*

Xiaofei Liu — Associate Processor, College of Chemistry and Chemical Engneering, Xinjiang Agricultural University, 311 East Nongda Road, 830052, Urumqi, China; e-mail: 1136887541@qq.com; https://orcid.org/0009-0000-9199-2989

Davronbek Bekchanov — Doctor of Chemical Sciences, Professor, Faculty of Chemistry, Department of Polymer Chemistry, National University of Uzbekistan, 100174, Tashkent, Uzbekistan; e-mail: bekchanovdj@gmail.com; https://orcid.org/0000-0002-3233-5572

Murzabek Ispolovich Baikenov — Doctor of Chemical Sciences, Professor, Karaganda Buketov University, Universitetskaya street, 28, 100024, Karaganda, Kazakhstan; e-mail: murzabek_b@mail.ru; https://orcid.org/0000-0002-8703-0397

Xintai Su (*corresponding author*) — Professor, School of Environment and Energy, Guangdong Provincial Key Laboratory of Solid Wastes Pollution Control and Recycling, South China University of Technology, 510006, Guangzhou, Guangdong, PR China; e-mail: suxintai@scut.edu.cn; https://orcid.org/0000-0001-6615-5273

Author Contributions

The manuscript was written through contributions of all authors. All authors have given approval to the final version of the manuscript. CRediT: **Xiaofei Liu** data curation, formal analysis, investigation, software, validation and writing — original draft; **Davronbek Bekchanov** software, resources and project administration; **Murzabek Ispolovich Baikenov** data curation, investigation, supervision and validation; **Xintai Su** conceptualization, funding acquisition, investigation, methodology, project administration, resources, supervision, visualization and writing-review and editing.

Conflicts of Interest

The authors declare no conflict of interest.

References

1 Ahmed, M., & Xinxin, G. (2016). A review of metal oxynitrides for photocatalysis. *Inorganic Chemistry Frontiers*, *3*(5), 578–590. https://doi.org/10.1039/c5qi00202h

2 Winikoff, S. G., & Cramer, C. J. (2014). Mechanistic analysis of water oxidation catalyzed by mononuclear copper in aqueous bicarbonate solutions. *Catal. Sci. Technol.*, *4*(8), 2484–2489. https://doi.org/10.1039/c4cy00500g

3 Zhang, X., Jia, X., Duan, P., Xia, R., Zhang, N., Cheng, B., Wang, Z., & Zhang, Y. (2021). V_2O_5/P-g-C_3N_4 Z-scheme enhanced heterogeneous photocatalytic removal of methyl orange from water under visible light irradiation. *Colloids and Surfaces A: Physicochemical and Engineering Aspects*, *608*, 125580. https://doi.org/10.1016/j.colsurfa.2020.125580

4 Fazli, S., & Asadpour-Zeynali, K. (2022). Investigation of electrochemical synthesis temperature effect of the binary transition metals sulfide on nickel foam in water oxidation study. *Materials Chemistry and Physics*, *291*, 126670. https://doi.org/10.1016/j.matchemphys.2022.126670

5 Wang, C., Xie, Z., deKrafft, K. E., & Lin, W. (2011). Doping Metal–Organic Frameworks for Water Oxidation, Carbon Dioxide Reduction, and Organic Photocatalysis. *Journal of the American Chemical Society*, *133*(34), 13445–13454. https://doi.org/10.1021/ja203564w

6 Chi, L., Xu, Q., Liang, X., Wang, J., & Su, X. (2016). Iron-Based Metal–Organic Frameworks as Catalysts for Visible Light-Driven Water Oxidation. *Small*, *12*(10), 1351–1358. Portico. https://doi.org/10.1002/smll.201503526

7 Kholdeeva, O. A., Skobelev, I. Y., Ivanchikova, I. D., Kovalenko, K. A., Fedin, V. P., & Sorokin, A. B. (2014). Hydrocarbon oxidation over Fe- and Cr-containing metal-organic frameworks MIL-100 and MIL-101–a comparative study. *Catalysis Today*, *238*, 54–61. https://doi.org/10.1016/j.cattod.2014.01.010

8 Wang, D., Wang, M., & Li, Z. (2015). Fe-Based Metal–Organic Frameworks for Highly Selective Photocatalytic Benzene Hydroxylation to Phenol. *ACS Catalysis*, *5*(11), 6852–6857. https://doi.org/10.1021/acscatal.5b01949

9 Zhang, X., Luo, J., Wan, K., Plessers, D., Sels, B., Song, J., Chen, L., Zhang, T., Tang, P., Morante, J. R., Arbiol, J., & Fransaer, J. (2019). From rational design of a new bimetallic MOF family with tunable linkers to OER catalysts. *Journal of Materials Chemistry A*, *7*(4), 1616–1628. https://doi.org/10.1039/c8ta08508k

10 Vaiano, V., Jaramillo-Paez, C. A., Matarangolo, M., Navío, J. A., & del Carmen Hidalgo, M. (2019). UV and visible-light driven photocatalytic removal of caffeine using ZnO modified with different noble metals (Pt, Ag and Au). *Materials Research Bulletin*, *112*, 251–260. https://doi.org/10.1016/j.materresbull.2018.12.034

11 Wang, P., Huang, B., Qin, X., Zhang, X., Dai, Y., Wei, J., & Whangbo, M. (2008). Ag@AgCl: A Highly Efficient and Stable Photocatalyst Active under Visible Light. *Angewandte Chemie International Edition*, *47*(41), 7931–7933. Portico. https://doi.org/10.1002/anie.200802483

12 Yan, X., Wang, X., Gu, W., Wu, M., Yan, Y., Hu, B., Che, G., Han, D., Yang, J., Fan, W., & Shi, W. (2015). Single-crystalline $AgIn(MoO_4)_2$ nanosheets grafted Ag/AgBr composites with enhanced plasmonic photocatalytic activity for degradation of tetracycline under visible light. *Applied Catalysis B: Environmental*, *164*, 297–304. https://doi.org/10.1016/j.apcatb.2014.09.046

13 Jung, H., Kim, C., Yoo, H.-W., You, J., Kim, J. S., Jamal, A., Gereige, I., Ager, J. W., & Jung, H.-T. (2023). Continuous-flow reactor with superior production rate and stability for CO_2 reduction using semiconductor photocatalysts. *Energy & Environmental Science*, *16*(7), 2869–2878. https://doi.org/10.1039/d3ee00507k

14 Ye, L., Liu, J., Gong, C., Tian, L., Peng, T., & Zan, L. (2012). Two Different Roles of Metallic Ag on Ag/AgX/BiOX (X = Cl, Br) Visible Light Photocatalysts: Surface Plasmon Resonance and Z-Scheme Bridge. *ACS Catalysis*, *2*(8), 1677–1683. https://doi.org/10.1021/cs300213m

15 Li, Q. F., Lu, K., Zhou, Q., & Baik, D. H. (2006). A study on interfacial mechanisms and structure of poly(ethylene-co-methacrylic acid)/copper with reflection–absorption infrared spectroscopy. *Journal of Materials Science*, *41*(24), 8271–8275. https://doi.org/10.1007/s10853-006-1006-7

16 Lyu, W., Shi, Y., Zheng, Y., & Liu, X. (2018). XPS and FTIR studies of fungus-stained Daemonorops margaritae. *Journal of Forestry Research*, *30*(2), 739–743. https://doi.org/10.1007/s11676-018-0598-5

17 Somvanshi, A., Ahmad, A., Husain, S., Manzoor, S., Qahtan, A. A. A., Zarrin, N., Fatema, M., & Khan, W. (2021). Structural modifications and enhanced ferroelectric nature of $NdFeO_3$–$PbTiO_3$ composites. *Applied Physics A, 127*(6). https://doi.org/10.1007/s00339-021-04562-1

18 Ling, D., Park, W., Park, S., Lu, Y., Kim, K. S., Hackett, M. J., Kim, B. H., Yim, H., Jeon, Y. S., Na, K., & Hyeon, T. (2014). Multifunctional Tumor pH-Sensitive Self-Assembled Nanoparticles for Bimodal Imaging and Treatment of Resistant Heterogeneous Tumors. *Journal of the American Chemical Society, 136*(15), 5647–5655. https://doi.org/10.1021/ja4108287